Journal of Process Control 154 (2025) 103527

Contents lists available at ScienceDirect

Journal of Process Control

journal homepage: www.elsevier.com/locate/jprocont

Non-linear control of a fuel gas blending benchmark problem with added consumer dynamics

M.D. Sibiya, A.J. Wiid, J.D. le Roux, I.K. Craig *

Department of Electrical, Electronic, and Computer Engineering, University of Pretoria, Pretoria, South Africa

ARTICLE INFO

Keywords:
Fuel gas blending
Model–plant mismatch
Moving horizon estimator
Non-linear model predictive control

ABSTRACT

This paper contributes to existing literature on fuel gas control by providing a feasible control solution with improved economic performance for an existing fuel gas control benchmark problem. Improved economic performance is achieved by implementing a non-linear model predictive controller (NMPC) that uses state estimates provided by a moving horizon estimator (MHE) and extended Kalman filter (EKF) for the fuel gas composition and flame speed index (FSI) to provide continuous inputs for the controller. Furthermore, the original fuel gas benchmark model is expanded to include consumer dynamics affecting fuel gas demand due to changes in the fuel gas heating value, making the model more representative of real industrial plants. The behaviour of an NMPC that neglects consumer dynamics ($NMPC_1$) was compared against an NMPC that includes consumer dynamics ($NMPC_2$).

The aim of the benchmark problem is to reduce the time-weighted average cost of fuel gas for three 46-hour cases, accounting for purchase costs and penalties for fuel gas specification violations. An optimal cost for each case is determined assuming ideal conditions and perfect control. The benchmark controller is a conventional multi-loop feedforward/feedback system and has an average cost for the three cases which is 38.5% higher than the optimal cost. The $NMPC_1$ controller has an average cost which is 33.9% higher than the optimal cost and better than the benchmark controller.

A new benchmark scenario was developed which includes the consumer dynamics. For the new scenario, $NMPC_1$ could not find a feasible solution, resulting in oscillations and specification violations. The oscillations would result in site-wide instabilities for all equipment using fuel gas. $NMPC_2$ was able to keep the process stable during these scenarios and maintain all specifications. This shows the necessity to include consumer dynamics for effective fuel gas blending control.

1. Introduction

Fuel gas serves as a major energy source in most chemical industrial plants. Typically, fuel gas consists of a blend of off-gases from downstream units. The off-gases are by-products or out-of-specification gas from downstream units which are flared if not used. If there is not a sufficient amount of off-gas to produce the necessary amount of fuel gas, additional gas such as Natural Gas (NG) must be purchased to make-up the deficiency. The optimisation objective of the fuel gas blending system is to use as much free off-gases as possible while maintaining various fuel gas quality specifications. Besides the obvious economic benefit, blending as much off-gases that are destined for flaring reduces total emissions as there is a reduction in burning of the purchased streams such as NG. Fuel gas blending control presents an interesting multivariable control opportunity due to the large number of consumers where small optimisation improvements can lead to significant environmental and financial benefits.

The modelling and control of industrial gas networks and headers have received increasing attention in the literature [1–6]. As far as fuel gas blending control is concerned, Dreyer and Kotze [7] has an active patent on the control of fuel gas blending, which covers methods and systems of controlling both a quantity metric (e.g., header pressure) and at least one quality metric (e.g. calorific value) of a fuel gas system. The methods include using non-linear equations to estimate fuel gas quality as well as using non-linear control with an extended Kalman filter (EKF) to compensate for unmeasured disturbances and model–plant mismatch. Brooks et al. [8] used the patented methods and software described by [7] to optimise the fuel gas blending system of a 90 000-bpd refinery in Cape Town, South Africa, as part of an overall Energy and Emissions Optimisation project.

Segers et al. [9] designed and installed a blending station to provide low cost blended natural gas to power plants in Odessa Texas. The plant

* Corresponding author.
E-mail address: ian.craig@up.ac.za (I.K. Craig).

https://doi.org/10.1016/j.jprocont.2025.103527
Received 31 March 2025; Received in revised form 8 July 2025; Accepted 7 August 2025
Available online 20 August 2025

blends cheaper high nitrogen (N_2) content (28%), low calorific value off-specification gas, with expensive high calorific value gas containing 2% N_2. The objective was to control the N_2 content below the gas turbine specification limit of 15% by installing a real-time fuel gas calorific analyser and controlling the flow rates of the two feed streams to achieve the optimal blend.

Muller et al. [10] modelled and validated an industrial fuel gas system and evaluated various control techniques. Traditional model predictive control (MPC) with static gains was compared to an Iterative MPC that updated the model gains every 10 min based on the developed first-principle non-linear models. Muller et al. [10] also evaluated implementing a real-time optimiser (RTO) in conjunction with the MPC. RTO involves using a non-linear steady-state optimiser to calculate optimal controlled variable (CV) targets and final manipulated variable (MV) resting values for the MPC. RTO provided the best economic performance for the scenario evaluated by [10], followed by the Iterative MPC.

Ricker et al. [11] expanded on the fuel gas system developed by [10] to include measurement limitations similar to what would be encountered in a real industrial plant. The system was developed into a benchmark problem that features three cases, each case consisting of 23 discrete events that occur over a 46-hour period. The benchmark solution provided by [11] involves using a non-linear solver to determine the optimal ratios of each feed stream required to maintain the fuel gas specifications, accounting for the maximum available feed rate of each stream. A total flow controller in the form of a conventional multi-loop feedforward/feedback system was used to maintain the pressure.

The effects of consumer dynamics was neglected by [10,11]. They modelled the effects on the header pressure from all the feed streams using the same transfer function which is not representative of real industrial plants as fuel gas demand flow rate ($F_{FG_{Demand}}$) is affected by the high heating value (HHV) of the fuel gas. The feed streams will cause different responses to $F_{FG_{Demand}}$ as the feed streams affect the HHV uniquely due to the difference in compositions. Sibiya et al. [12] modelled these effects using a furnace as consumer which is under Proportional-Integral (PI) feedback control together with a Smith predictor for dead-time compensation. They highlighted the effects of model–plant mismatch when using a linear MPC that neglects the consumer dynamics. Models linearised at nominal conditions were used to represent the fuel gas blending process.

Although the benchmark problem [11] was published more than a decade ago, there have been no published attempts to improve the performance. The main contribution of this paper is to provide a control solution which improves on the original controller tested on the benchmark problem. The control solution relies on providing continuous, accurate predictions of the fuel gas composition in the presence of measurement errors and limitations encountered in the benchmark problem, using an EKF and MHE. The composition predictions are then used in a non-linear MPC (NMPC) to control the fuel gas system.

Furthermore, this paper expands on the work done in [12] by incorporating consumer dynamics into the non-linear model used in the benchmark problem [11], making it more representative of a real industrial plant. The behaviour of two NMPCs is investigated, one that neglects consumer dynamics and another that includes the consumer dynamics in the controller state equations. It is shown that with limitations in the feed supply streams, the NPMC which considers the additional consumer dynamics is able to solve for a feasible and stable solution where all CVs are within limits. The NMPC which does not include consumer dynamics did not find a feasible solution and exhibited unstable oscillatory behaviour.

The paper is organised as follows. Section 2 summarises the fuel gas blending process and models and presents the additional consumer dynamic models. Section 3 details the available measurements for the process. Section 4 explains the cost function used to evaluate the economic performance of the benchmark problem. Section 5 develops a state estimator for the fuel gas composition as well as flame speed index (FSI) to be used by the NMPC. Section 6 explains the NMPC design and tuning. Section 7 presents the NMPC results to the benchmark problem. Section 8 presents a new case that includes consumer dynamics and the results of two NMPCs in the presence of the consumer dynamics: $NMPC_1$ which excludes the consumer dynamics versus $NMPC_2$ which accounts for these. Section 9 concludes the paper.

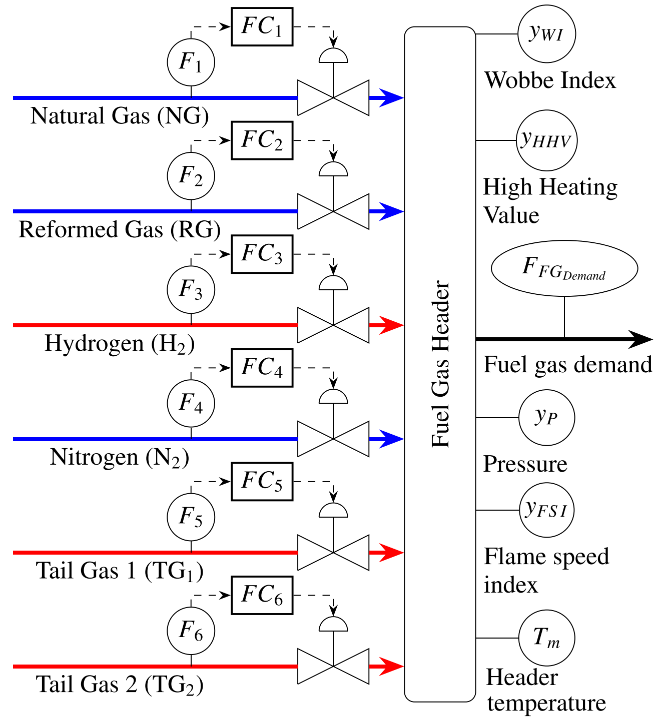

Fig. 1. Process diagram of fuel gas header with purchase streams in blue and off-gases in red.

2. Process overview

This section gives an overview of the fuel gas system and the process models developed by [10], and used in the fuel gas blending benchmark problem [11]. The consumer dynamics developed in [12] are also presented. Fig. 1 shows the process diagram of the system.

2.1. Process description

The fuel gas system blends six feed streams (F_i), namely, NG (F_1), reformed gas (RG) (F_2), hydrogen (H_2) (F_3), N_2 (F_4), tail gas 1 (TG_1) (F_5), and tail gas 2 (TG_2) (F_6). The aim is to keep the header pressure (y_P) within limits while maintaining the fuel gas specifications. These specifications are the fuel gas HHV (y_{HHV}), the Wobbe Index (WI) (y_{WI}), and FSI (y_{FSI}). A header temperature measurement (T_m) is available, but it is not controlled. Table 1 shows the fuel gas system operating ranges and costs.

NG and N_2 are purchased make-up streams. NG is rich in hydrocarbons (methane (CH_4) and heavier hydrocarbons (C_2^+)) and is primarily used to keep the calorific value (y_{HHV}) of the fuel gas above the minimum specification. NG comes from multiple sources and the stream composition changes in a stepwise manner when the industrial plant switches sources [10,11].

N_2 has no calorific value and is typically used during high y_{FSI} periods to maintain y_{FSI} below the high limit. The N_2 stream has a constant high composition purity (~100%). RG is the synthesis gas intended to be used by downstream units to produce valuable products. NG, RG, and N_2 have costs associated with their usage.

Table 1
Fuel gas operating range and stream costs.

	Min	Max	Unit	Relative Cost [Cost/kNm^3]
Inputs (MVs)				
NG (F_1)	0	15	kNm^3/h	0.678
RG (F_2)	0	20	kNm^3/h	0.254
H_2 (F_3)	0	5	kNm^3/h	0
N_2 (F_4)	0	5	kNm^3/h	0.068
TG_1 (F_5)	0	30	kNm^3/h	0
TG_2 (F_6)	0	30	kNm^3/h	0
Outputs (CVs)				
y_{HHV}	16.5	18	MJ/Nm^3	–
y_{WI}	25	27	MJ/Nm^3	–
y_{FSI}	39	46	–	–
y_P	2 000	2 200	kPa	–

TG_1 and TG_2 are off-gases from downstream units within the industrial plant that are flared if not blended in the fuel gas. The composition of TG_1 and TG_2 typically varies continuously which disturbs the process. The H_2 stream is excess hydrogen not used downstream and is bound for flaring. Its composition is constant (assumed 100% pure). These three streams have no direct costs when used within the fuel gas blending system. The availability of the three streams varies based on operations and can sometimes drop to zero. RG is typically used in the fuel gas system when TG_1 and/or TG_2 are unavailable.

The feed stream flow rates are MVs, and $F_{FG_{Demand}}$ is a measured disturbance variable. $F_{FG_{Demand}}$ is dependent on downstream fuel gas consumers within the industrial plant. These are typically furnaces, fired heaters and boilers [8,13]. In a real industrial plant, $F_{FG_{Demand}}$ is also affected by y_{HHV}. If y_{HHV} decreases, the consumers increase $F_{FG_{Demand}}$ to maintain the same fuel gas demand duty (Q_{Demand}) [11,12]. These dynamics are not present in the original benchmark problem [11].

The optimisation objective is to use as much off-gases as possible while maintaining the quality specifications and $F_{FG_{Demand}}$. Increasing the use of off-gases results in the reduction of expensive make-up gas purchases and reductions in total gases flared across the plant.

2.2. Process models

The process models of the fuel gas system were developed and validated using data from an industrial plant by [10].

The system can be described using six states which are the moles of the six chemical components present in the fuel gas. These components are CH_4, C_2^+, H_2, N_2, carbon monoxide (CO) and carbon dioxide (CO_2). The state equations based on the mass balance, assuming perfect mixing and no reactions, are [11]

$$\frac{dN_j}{dt} = 44.64 \sum_{i=1}^{6} \left(y_{ji} F_i - y_j F_{FG_{Demand}} \right), \tag{1}$$

where index i refers to the six feed streams, index j refers to the chemical components, and N_j [kmol] is the molar amount of j in the header. F_i and $F_{FG_{Demand}}$ are measured in units of kNm^3/h, and must be multiplied by 44.64 to convert from kNm^3/h to kmol/h [10,11]. y_{ji} is the mole fraction of component j in stream i. Table 2 gives the typical y_{ji} values of each feed stream. y_j is the mole fraction of component j in the header calculated as

$$y_j = \frac{N_j}{N_T}, \tag{2}$$

where N_T [kmol] is the total number of moles in the header ($\sum_{j=1}^{6} N_j$).

Using the ideal gas law, the pressure y_P [kPa] of the fuel gas header is calculated as

$$y_P = \frac{N_T R T Z}{V}, \tag{3}$$

where $V = 100$ m^3 is the fuel gas header volume, Z is the compressibility factor assumed to be 1.06, $R = 8.314$ J/mol·K is the universal gas constant and T [K] is the header temperature [11].

The gas properties for the fuel gas are calculated based on the molar compositions [10,11]. y_{HHV} [MJ/Nm^3] is calculated as

$$y_{HHV} = \sum_{j=1}^{6} y_j HHV_j, \tag{4}$$

where HHV_j [MJ/Nm^3] is the HHV of component j given in Table 3 [10]. y_{WI} [MJ/Nm^3] is calculated as

$$y_{WI} = \frac{y_{HHV}}{\sqrt{\rho_{FG}}}, \tag{5}$$

where ρ_{FG} is the specific gravity of the fuel gas, calculated as

$$\rho_{FG} = \frac{\sum_{j=1}^{6} y_j MW_j}{MW_{air}}, \tag{6}$$

where MW_j [kg/kmol] is the molar weight of component j, and $MW_{air} = 28.8$ [kg/kmol] is the molar weight of air [10]. y_{FSI} is calculated as

$$y_{FSI} = \frac{\sum_{j=1}^{6} y_j s_j}{\sum_{j=1}^{6} y_j A_j + 5(y_{N_2} + y_{CO}) + 1}, \tag{7}$$

where s_j is the flame speed factor and A_j is the molar stoichiometric air demand factor of component j. y_{N_2} and y_{CO} are the mole fractions of N_2 and CO_2 respectively. N_2 and CO_2 are treated as inert gasses. The component characteristics are given in Table 3.

2.3. Consumer dynamics model

Detailed modelling of the fuel gas consumer dynamics is described in [12]. The dynamics are based on furnace behaviour under coil outlet temperature PI control with a Smith predictor for dead-time compensation. This model is chosen because furnaces and other fired heaters represent up to 90% of the fuel gas usage of a refinery [13]. The control objective is to control the temperature of a process outlet stream at a desired value by manipulating fuel gas demand going into the burners which will then vary the furnace duty to achieve the desired outlet temperature. y_{HHV} is a disturbance to the furnace and influences the amount of $F_{FG_{Demand}}$ required to maintain the desired outlet temperature.

The changes in $F_{FG_{Demand}}$ due to consumer dynamics caused by changes in y_{HHV} will have secondary effects on y_P. Since all the different streams cause different effects to y_{HHV}, the secondary effects will be different for all streams. Table 4 shows the models for changes in $F_{FG_{Demand}}$ for the six fuel gas feed streams linearised at the nominal fuel gas conditions [12]. Table 4 also shows the linearised y_P models from [10] which exclude the consumer dynamics (y_{P1}) and those from [12] which include the consumer dynamics (y_{P2}) at the nominal conditions. Sibiya et al. [12] showed that the largest consumer dynamics effects would be on the NG and N_2 streams.

The relationship between $F_{FG_{Demand}}$ and y_{HHV} can be derived from the furnace control scheme block diagram shown in [12]. After model order reduction, the relationship is given by

$$\frac{F_{FG_{Demand}}(s)}{y_{HHV}(s)} = \frac{k}{(1 + 0.45s)}, \tag{8}$$

where k is the gain calculated based on the current y_{HHV} and $F_{FG_{Demand}}$. This model will be used in the controller implementation to represent the consumer dynamics.

Table 2
Typical compositions (y_{ij}) and properties for the feed streams (F_i).

	j	NG (F_1)	RG (F_2)	H_2 (F_3)	N_2 (F_4)	TG_1 (F_5)	TG_2 (F_6)
CH_4	1	0.911	0.015	–	–	0.055	0.15
C_2^+	2	0.068	0.0	–	–	0.01	0.01
H_2	3	0.0	0.62	1	–	0.62	0.57
N_2	4	0.015	0.005	–	1	0.025	0.06
CO	5	0.0	0.31	–	–	0.26	0.13
CO_2	6	0.006	0.05	–	–	0.03	0.08
HHV [MJ/Nm^3]		43.02	11.78	12.10	0.0	13.96	15.39
WI [MJ/Nm^3]		52.62	17.87	45.73	0.0	21.60	22.92

Table 3
Component characteristics.

	j	HHV_j [MJ/Nm^3]	WI_j [MJ/Nm^3]	ρ_j	MW_j [kg/kmol]	A_j	s_j
CH_4	1	37.78	50.72	0.557	16.04	9.55	148
C_2^+	2	126.5	87.62	2.018	58.12	31.0	514
H_2	3	12.10	45.88	0.069	2.02	2.39	339
N_2	4	–	–	0.973	28.02	–	–
CO	5	11.97	12.17	0.968	28.01	2.39	61
CO_2	6	–	–	1.528	44.01	–	–

Table 4
Fuel streams to fuel gas demand models [10,12]. y_{P1} excludes consumer dynamics and y_{P2} includes consumer dynamics.

	NG (F_1)	RG (F_2)	H_2 (F_3)	N_2 (F_4)	TG_1 (F_5)	TG_2 (F_6)
$F_{FG_{Demand}}$	$\frac{-1.5e^{-2.25s}}{0.905s^2+2.54s+1}$	$\frac{0.332e^{-2.25s}}{1.11s^2+3.04s+1}$	$\frac{0.332e^{-2.25s}}{0.97s^2+2.71s+1}$	$\frac{1e^{-2.25s}}{1.12s^2+3.05s+1}$	$\frac{0.223e^{-2.25s}}{0.992s^2+2.77s+1}$	$\frac{0.127e^{-2.25s}}{1.15s^2+3.09s+1}$
y_{P1}	$\frac{18.67}{s}$	$\frac{18.67}{s}$	$\frac{18.67}{s}$	$\frac{18.67}{s}$	$\frac{18.67}{s}$	$\frac{18.67}{s}$
y_{P2}	$\frac{46.8}{s(2.92s+1)}$	$\frac{12.7(4.52s+1)}{s(1.1s+1)^2}$	$\frac{12.7(4.35s+1)}{s(1.09s+1)(s+1)}$	$\frac{106}{(3.03s+1)(0.21s+1)}$	$\frac{14.7(3.09s+1)}{s(0.96s+1)(0.85s+1)}$	$\frac{16.5(2.14s+1)}{s(0.77s+1)(0.73s+1)}$

Table 5
Summary of available measurements in the benchmark problem [11].

	Description	Unit	Sample Interval (s)	Delay (s)	σ
$F_{i,max}$	Feed stream maximum availability	kNm^3/h	20	0	0
$F_{FG_{Demand}}$	Fuel gas demand flow rate	kNm^3/h	20	0	0.9
T_m	Header temperature	K	20	0	0
y_P	Header pressure	kPa	20	0	5
y_{HHV}	Fuel gas high heating value	MJ/Nm^3	20	20	0.07
y_{WI}	Fuel gas Wobbe index	MJ/Nm^3	20	60	0.07
y_{FSI}	Fuel gas flame speed index	–	600	120	0.07
y_{i_s}	Mole fraction for stream indicated by i_s	mol%	600	120	0
i_s	Spectrometer stream status indicator	–	120	0	0

3. Measurements

The measurements on the benchmark problem [11] are representative of what would be encountered on an industrial plant. All measurements, except the mass spectrometer analyser, have a sampling period of 20 seconds. All flows, y_P, and T_m measurements have negligible dead-time. y_{HHV} and y_{WI} have dead-times of 20 seconds and 1 minute respectively.

A single mass spectrometer is used to measure the five streams that have varying compositions (NG, RG, TG_1, TG_2 and Fuel gas) in Fig. 1. (In other words, it measures y_{ij} for the NG, RG, TG1 and TG2 streams, and y_j for the fuel gas stream.) Each stream takes 2 min to analyse. Therefore, the sampling period for each stream is 10 minutes and the measurement will be 2 minutes delayed. The analyser has a status indicator i_s to indicate which stream has the latest available measurement. There is a 0.001 probability that a bad measurement can occur [11]. If a bad measurement does occur, i_s shows a negative number. y_{FSI} is calculated based on the mass spectrometer; therefore, it only updates every 10 min.

The analyser cannot give the exact composition of the C_2^+ component and only gives the total C_2^+ fraction. Because the actual C_2^+ is time-varying, the measured y_{HHV} and y_{WI} can differ from those calculated using the analyser composition.

All measurements have systematic calibration errors and noise approximated using the standard deviation σ of each signal when at steady-state. Table 5 summarises the measurements.

4. Economic performance evaluation formula

The economic objective of the fuel gas system is to minimise the cost of gas purchasing while maintaining the demand and specifications. The instantaneous cost (C), therefore, is a combination of two parts: the cost of the streams per demand (C_c) and the penalty incurred for specification violations (C_δ) [11],

$$C = C_c + C_\delta. \tag{9}$$

Detailed explanation and equations to calculate the costs are given in [11]. The performance metric for each case is taken as the averaged cost $\bar{C}$ over the 46-hour case period. $\bar{C}$ at a discrete time instant $t_k > 0$ is taken as

$$\bar{C}(t_k) = \frac{\sum_{j=1}^{k} C(t_j)}{k}. \tag{10}$$

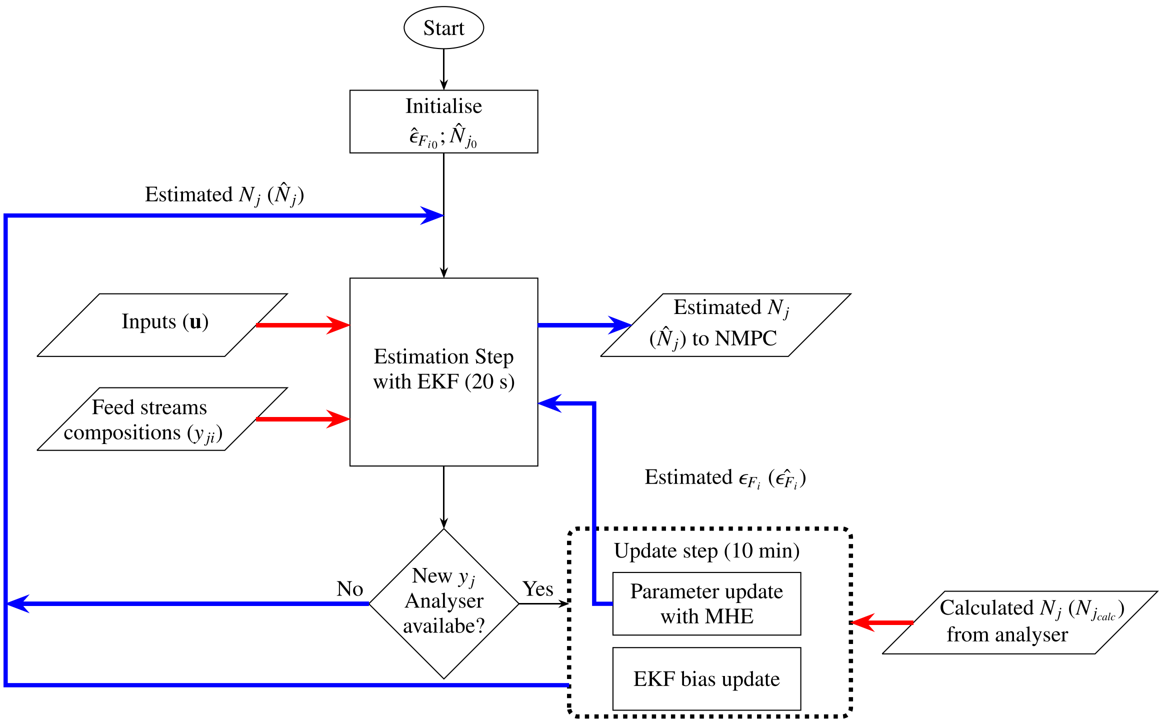

Fig. 2. Flowchart of fuel gas estimator implementation with input variables in red and estimated variables in blue.

Ricker et al. [11] provides optimal costs ($C_{Optimal}$) for each of the three benchmark test cases. The optimal costs were calculated under ideal conditions (accurate, noise-free and continuous measurements of all gas compositions and specifications). Small constraint violations were not penalised when calculating the optimal costs. $C_{Optimal}$ represents the best possible costs that could be achieved with perfect control.

5. Fuel gas composition estimator

To improve the performance of any control scheme that relies on the composition of the fuel gas, a continuous measurement of the composition is beneficial. Since the fuel gas composition is only updated every 10 min (assuming a bad status indication does not occur), an estimator can be used to provide continuous estimates of the fuel gas moles ($\hat{N}_j$) and composition ($\hat{y}_j$).

5.1. Estimator selection

Given accurate measurements of F_i, $F_{FG_{Demand}}$ and y_{ji}, the fuel gas composition can be continuously estimated using (1), (2) and a state estimator such as an extended Kalman filter (EKF). Bias updates could then be made to the estimates every 10 min when the fuel gas analyser updates.

The biggest challenge with implementing a fuel gas composition estimator for the benchmark fuel gas system is the presence of calibration errors (ϵ_{F_i}) on the flow rate measurements. This is an important issue in blending applications and prevents accurate prediction of compositions using mass balance due to the actual F_i of each stream ($F_{i_{actual}}$) not being known. The calibration errors on the flow rates of the benchmark system are representative of industrial plants, unknown, and different for each case [11]. The calibration errors are additive and $F_{i_{actual}}$ is given as

$$F_{i_{actual}} = F_i + \epsilon_{F_i}. \tag{11}$$

The $F_{i_{actual}}$ measurements differ from the controller outputs and are not available for use in the implementation of the control solution. Using just an EKF to predict the fuel gas composition fails due to the presence of the calibration errors. To overcome this limitation, a moving horizon estimator (MHE) was implemented together with an EKF. The MHE is used every 10 min to estimate the calibration errors and provide these estimates to the EKF, which runs every 20 s to better predict the fuel gas composition.

The EKF calculates $\hat{N}_j$ based on estimated ϵ_{F_i} ($\hat{\epsilon_{F_i}}$) values. The EKF uses $\hat{\epsilon_{F_i}}$ together with the F_i signals from the controller to calculate $F_{i_{actual}}$, which is then used in place of F_i in (1) to estimate the fuel gas composition. The MHE uses N_{MHE} previous analyser updates together with the EKF estimations to update $\hat{\epsilon_{F_i}}$. $\hat{\epsilon_{F_i}}$ is obtained by minimising the squared sum of the estimate errors from the past measurements (arrival cost). Fig. 2 shows a flowchart of the estimator implementation.

Various methods to compute the arrival cost in the MHE framework have been studied, such as Kalman filters for linear systems [14] and extended Kalman filters for non-linear systems [15]. Other methods to compute the arrival cost include unscented Kalman filtering [16], sampling based filters [17], particle filters [18], nonlinear programming (NLP) sensitivity [19], adaptive estimation methods [20] and a recursive approach [21]. For this study, the EKF method provided satisfactory results.

5.2. Estimator implementation

The estimator is divided into two steps: an estimation step that calculates $\hat{N}_j$ at every execution interval (20 s) using an EKF, and an update step that biases $\hat{N}_j$ on the EKF and updates $\hat{\epsilon_{F_i}}$ using the MHE every 10 min when new fuel gas analyser values become available.

5.2.1. Estimation step

For the estimation step, a state-space model of N_j for the EKF was obtained by linearising (1) around the nominal operating point and discretising (1) using Euler's method with a step-size of 2 s. For the model, the states are $x_j = N_j$, the inputs are $\mathbf{u} = \left[F_{FG_{Demand}},\ F_i\right]^T$, and the parameters are $\mathbf{p} = \left[y_{ji},\ \hat{\epsilon_{F_i}}\right]^T$. $\hat{\epsilon_{F_i}}$ is initialised as $[0, 0, 0, 0, 0, 0]^T$ and subsequently updated with the MHE when the mass spectrometer

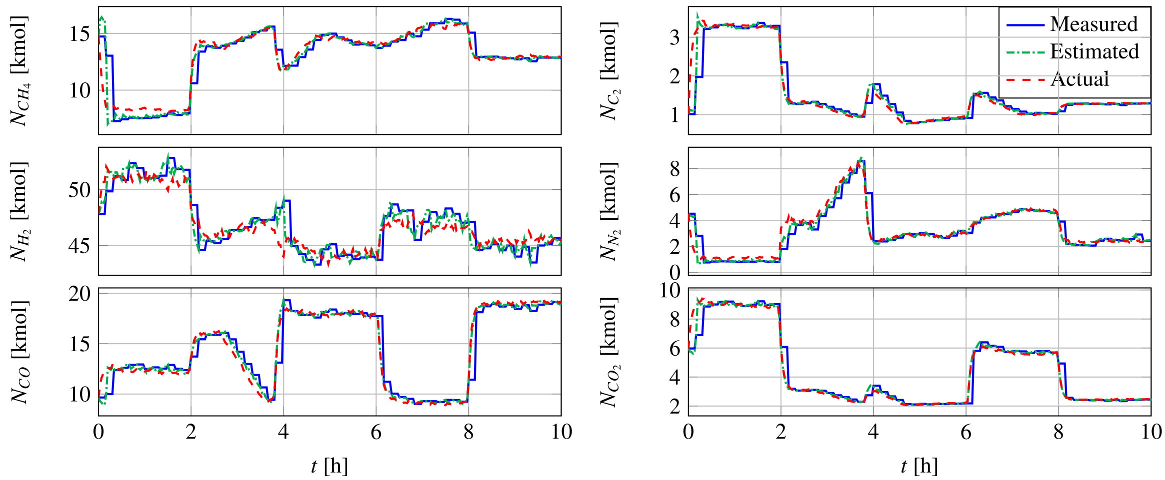

Fig. 3. Comparison of estimated states against actual and measured states.

measurements of y_{ji} becomes available every 10 min. The full state vector is measured. The initial states are calculated at the nominal values of the benchmark as $[14.73, 1.01, 47.81, 4.52, 9.66, 5.97]^T$.

5.2.2. Update step

The fuel gas analyser measures the mole fraction y_j in mol%, whereas the MHE provides the state estimates ($\hat{N}_j$) as kmol. The molar amount N_j can be calculated using (3) such that:

$$N_{j_{calc}} = y_j N_T = y_j \frac{y_P V}{RT_m Z}. \tag{12}$$

$N_{j_{calc}}$ is then used during the EKF and MHE update step.

The MHE problem is formulated as:

$$\min_{\hat{\epsilon}_{F_i}} \; J_{MHE} \tag{13}$$

subject to,

$$\hat{N}_j(t_{k-i|k}) \geq 0, \quad \forall \; i = 0, 1, \ldots, N_{MHE}, \tag{14a}$$

$$-1 \leq \hat{\epsilon}_{F_i} \leq 1, \tag{14b}$$

where

$$J_{MHE} = \left\| \Delta\hat{\epsilon}_{F_i}(t_k) \right\|^2 W_{\hat{\epsilon}_{F_i}} + \sum_{i=0}^{N_{MHE}} \left\| \hat{N}_{j_{delayed}}(t_{k-i|k}) - N_{j_{calc}}(t_{k-i|k}) \right\|^2 W_Y. \tag{15}$$

N_{MHE} is the estimation horizon which is the number of previous measured values to use when estimating $\hat{\epsilon_{F_i}}$. N_{MHE} was taken as 20. $\hat{N}_{j_{delayed}}$ is $\hat{N}_j$ from 2 min prior to the analyser update, since the analyser update is only available after a 2 min delay. The time between each sampling interval t_k is 10 min. $\Delta\hat{\epsilon}_{F_i}$ is the change in $\hat{\epsilon}_{F_i}$ from the previous estimates. $W_{\hat{\epsilon_{F_i}}}$ and W_Y are weighting matrices. $W_{\hat{\epsilon_{F_i}}}$ was set as 0 and W_Y was set as $I_{6\times6}$.

5.3. Composition state estimation results

Fig. 3 shows the results of the estimator against the actual N_j for the first 10 h of case 1 of the benchmark problem. The estimates initially start with a larger deviation to the actual N_j, which is due to the presence of the calibration errors in the flow measurements. As more measurements become available and the MHE is able to better predict $\hat{\epsilon_{F_i}}$, the estimates become more accurate until they closely match the actual N_j.

5.4. FSI estimation

y_{FSI} has a 10 min update interval as it is based on the fuel gas analyser readings. To provide a continuous measurement for improved control, the estimated fuel gas compositions together with (7) is used to provide a continuous estimate of y_{FSI} ($\hat{y}_{FSI}$).

The controller will have $\hat{y}_{FSI}$ as the CV rather than the less frequently available y_{FSI}. $\hat{y}_{FSI}$ does not need to be biased using the actual y_{FSI} since the composition estimates used to calculate $\hat{y}_{FSI}$ are already biased using the analyser measurements (Section 5.2.2).

Fig. 4 shows $\hat{y}_{FSI}$ against the actual y_{FSI} for case 1 of the benchmark [11]. Similar to the state estimates, $\hat{y}_{FSI}$ starts with a large deviation but becomes more accurate as more measurements become available to better estimate $\hat{\epsilon_{F_i}}$ and the states. The close match between $\hat{y}_{FSI}$ and y_{FSI} shows that the controller can use the estimates to maintain the y_{FSI} specification. The actual y_{FSI} will still be used for the performance evaluation in the benchmark.

6. NMPC design

This section describes the development of the NMPC that uses the measurements discussed in Section 3, and the estimates discussed in Section 5 to control the fuel gas system. NMPC was chosen because the fuel gas system is non-linear, and the process gains for all specifications change depending on the current composition of the fuel gas header and the feed streams.

6.1. NMPC model state function

The NMPC model is based on the models described in Section 2.2. No offset-free mechanism is implemented in this article.

6.1.1. NMPC model state function variables

The state $\mathbf{x}$, input $\mathbf{u}$, and the output $\mathbf{y}$ vectors are defined as:

$$\mathbf{x} = [\hat{N}_1, \hat{N}_2, \hat{N}_3, \hat{N}_4, \hat{N}_5, \hat{N}_6]^T, \tag{16a}$$

$$\mathbf{u} = [F_1, F_2, F_3, F_4, F_5, F_6]^T, \tag{16b}$$

$$\mathbf{y} = [y_{HHV}, y_{WI}, \hat{y}_{FSI}, y_P]^T. \tag{16c}$$

The upper limits of the inputs are changed online during run time by using the available $F_{i,max}$ signals.

NG, RG, TG_1, TG_2 compositions and T_m are considered as parameters and updated during the controller run time by directly using their measurements when they become available as described in Section 3.

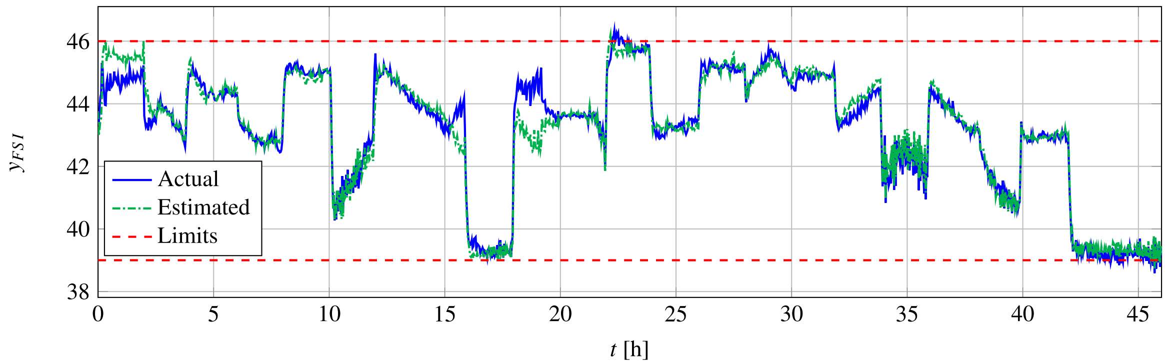

Fig. 4. Comparison of estimated FSI against actual FSI.

The N_2 and H_2 feed streams are assumed as pure components with a constant composition of 100%. The parameter vector $\mathbf{p}$ is defined as

$$\mathbf{p} = [y_{1j}, y_{2j}, y_{5j}, y_{6j}, T_m]^T. \tag{17}$$

6.1.2. NMPC cost function

The NMPC problem is formulated as:

$$\min_{\mathbf{u}(k+1|k),\ldots,\mathbf{u}(N_c+1|k)} J_{NMPC} \tag{18}$$

subject to:

$$\mathbf{x} \in \mathbb{R}^{N_x \times N_p}, \quad \mathbf{x} \geq 0; \tag{19a}$$

$$\mathbf{y} \in \mathbb{R}^{N_y \times N_p}, \quad \underline{\mathbf{y}} \leq \mathbf{y} \leq \bar{\mathbf{y}}; \tag{19b}$$

$$\mathbf{u} \in \mathbb{R}^{N_u \times N_c}, \quad \underline{\mathbf{u}} \leq \mathbf{u} \leq \bar{\mathbf{u}}; \tag{19c}$$

$$\boldsymbol{\Delta}\mathbf{u} \in \mathbb{R}^{N_u \times N_c}, \quad \Delta\underline{\mathbf{u}} \leq \boldsymbol{\Delta}\mathbf{u} \leq \Delta\bar{\mathbf{u}}; \tag{19d}$$

$$\mathbf{x}(k+i+1|k) = f_k\left(\mathbf{x}(k+i|k), \mathbf{u}(k+i|k), \mathbf{p}(k+i|k)\right), \tag{19e}$$

$$\mathbf{y}(k+i|k) = g_k\left(\mathbf{x}(k+i|k), \mathbf{p}(k+i|k)\right), \quad \forall i = 1, 2, \ldots, N_p. \tag{19f}$$

where

$$J_{NMPC} = \sum_{i=1}^{N_P} \|\mathbf{y}(k+i|k) - \mathbf{r}^{\mathbf{y}}(k+i)\|^2 \mathbf{W_P} + \sum_{i=1}^{N_C} \left(\|\boldsymbol{\Delta}\mathbf{u}(k+i|k)\|^2 \mathbf{W_C} + \|\mathbf{u}(k+i|k) - \mathbf{r}^{\mathbf{u}}(k+i)\|^2 \mathbf{W_L} \right). \tag{20}$$

N_P is the prediction horizon and N_C is the control horizon. (1) is used to calculate the states (f_k) and (3) to (7) are used to calculate the outputs (g_k). $\mathbf{W_P}$, $\mathbf{W_C}$, and $\mathbf{W_L}$ are weighting matrices for the output reference error, input move sizes and input deviations from their references respectively. The references $\mathbf{r^y}$ and $\mathbf{r^u}$ are the desired output and input trajectories respectively. $\underline{\mathbf{y}}$ and $\bar{\mathbf{y}}$ are the output low and high limits, $\underline{\mathbf{u}}$ and $\bar{\mathbf{u}}$ are the input low and high limits, and $\Delta\underline{\mathbf{u}}$ and $\boldsymbol{\Delta}\bar{\mathbf{u}}$ are the change in input low and high limits. The NMPC follows a receding horizon approach.

6.2. NMPC tuning

This section details the tuning used for the NMPC. The controller is implemented using the MATLAB MPC toolbox [22]. The final NMPC tuning parameters are given in Table 6. The controller sampling time (T_s) was chosen as 20 s, and N_P was chosen as 15 samples (5 min). N_C was chosen with blocking implemented at intervals [1 1 2 3 5 3] which means that the controller only calculates moves for the 1st, 2nd, 4th, 7th, 12th and 15th (last) interval in the predicted horizon. Blocking ensures the controller is robust and does not make aggressive moves [22].

Table 6
Final NMPC variable tuning parameters.

	Min	Max	Scale Factor	Weight	Rate Weight
			Inputs (MVs)		
NG	0	15	30	67.8	5
RG	0	20	30	25.4	5
H_2	0	5	30	0	5
N_2	0	5	30	6.8	5
TG_1	0	30	30	0	5
TG_2	0	30	30	0	5
			Outputs (CVs)		
y_{HHV}	16.5	18	1.5	10	–
y_{WI}	25	27	2	10	–
y_{FSI}	39	46	7	10	–
y_P	2 000	2 200	200	15	–

No Δu limits are implemented to give the controller freedom. To reduce excessive MV movements observed during the benchmark cases, $\mathbf{W_C}$ is chosen as,

$$\mathbf{W_C} = \mathbf{S_U^{-1}} 5 \mathbf{I_{6\times6}} \tag{21}$$

where $\mathbf{S_U^{-1}}$ is the diagonal MV scaling matrix MATLAB uses to scale the MVs. The scaling for all MVs is given as 30, which corresponds with the largest range for the TG_1 and TG_2 streams.

To optimise the economic cost of fuel gas, $\mathbf{r^u}$ and $\mathbf{W_L}$ are chosen as,

$$\mathbf{r^u} = [0, 0, 5, 0, 30, 30]^T, \tag{22a}$$

$$\mathbf{W_L} = \mathbf{S_U^{-1}} \mathrm{diag}\,(67.8,\ 25.4,\ 0,\ 6.8,\ 0,\ 0). \tag{22b}$$

The MVs associated with NG, RG and N_2 are given targets of 0 to minimise them and weights of 67.8, 25.4 and 6.8, respectively, in proportion to their relative costs provided in Table 1. The MV high limit values are changed online based on the benchmark $F_{i,max}$ signals.

For the CVs, $\mathbf{r^y}$ and $\mathbf{W_P}$ are chosen as,

$$\mathbf{r^y} = [17.25, 26, 42.5, 2100]^T, \tag{23a}$$

$$\mathbf{W_P} = \mathbf{S_Y^{-1}} \mathrm{diag}(10,\ 10,\ 10,\ 15). \tag{23b}$$

where $\mathbf{S_Y^{-1}}$ is the diagonal CV scaling matrix. The scaling factor was taken as the range for each CV. Since the control objective of the fuel gas blending benchmark is to keep the CVs within the limits and not setpoint control, $\mathbf{r^y}$ is chosen as the middle values of the CV ranges. All CVs have the same weights, except for y_P, which is given a larger weight so that the controller moves the pressure away from the low limit towards the midpoint.

As can be expected, NMPC tuning parameters influences the controller behaviour and performance, specifically the achieved cost. The final parameters presented in the article were obtained through trial-and-error and yielded the best overall results. Potentially better tuning parameters can be obtained to improve the final cost, but the current parameters give a satisfactory performance across all the different cases.

A stability analysis of the closed-loop system is considered outside the scope of this study. In an industrial plant there is generally a fall-back local controller which takes over should the NMPC misbehaves.

7. Benchmark results

The NMPC is applied to the three benchmark cases defined in [11]. Each benchmark case is 46 h long and has 23 unique discrete upsets, each occurring every 2 h. The feed streams gas compositions vary gradually over time, and each case has different biases for the feed streams flow measurements. Neither the simulated plant or the controller model include consumer dynamics. In this section, the results of the NMPC are presented for case 1 of the benchmark. Table 7 presents a summary of the results for all the three cases.

7.1. Case 1 performance

Figs. 5 and 6 show the response of the controller for the first benchmark case. The last row of Fig. 6 shows the instantaneous economic cost and time-weighted average cost. The optimal costs, as provided in the benchmark results, are plotted as dotted green lines. As expected, C and $\bar{C}$ in Fig. 6 for both the NMPC and the optimal solution increases when there is a reduction of TG_1 and TG_2 availability.

Fig. 6 shows that the controller generally keeps the CVs within limits while also being close to $C_{Optimal}$. y_{WI} is on or below the low specification limit of 25 for extended periods. y_{HHV} is also frequently on or above the high specification limit. There are also a few instances when y_{FSI} and y_P violate their limits.

Unlike $C_{Optimal}$, the NMPC cost C has spikes when it violates the specification limits, especially between 10–20 and 34–46 h. The spikes in C are mostly due to violations of the y_{WI} and y_{HHV} limits at those times. The limits could be adjusted for the CVs but this would affect the optimal solution that the controller calculates and could ultimately result in reduced performance in other scenarios.

7.2. Summary of all benchmark cases

Table 7 shows the final $\bar{C}$ as well as the contribution of $\bar{C}_\delta$ to the final $\bar{C}$ for each of the cases. For case 1, $\bar{C}_\delta$ contributes 15.3% to the total $\bar{C}$ of 0.1132. $\bar{C}$ for case 1 is 45.1% higher than $\bar{C}_{Optimal}$. This is a big improvement from the benchmark controller, which is 70.6% higher than $\bar{C}_{Optimal}$.

Although the controller provided a significant improvement for case 1, case 2 had a poorer performance and case 3 had a fairly similar performance to the benchmark controller. The response of the controller for case 2 and 3 are not shown due to space limitations. For case 2, $\bar{C}_\delta$ contributes 8.9% to the total cost $\bar{C}$ of 0.1128. $\bar{C}$ for case 2 is 29.7% higher than $\bar{C}_{Optimal}$. This is a decrease in performance from the benchmark controller, which is 19.1% higher than $\bar{C}_{Optimal}$.

For case 3, $\bar{C}_\delta$ contributes 3.5% to the total cost $\bar{C}$ of 0.0941. $\bar{C}$ for case 3 is 27.2% higher than $\bar{C}_{Optimal}$. This is a slight increase in performance from the benchmark controller, which is 27.6% higher than $\bar{C}_{Optimal}$.

Overall, the NMPC performs better than the benchmark controller, achieving an average cost that is 33.9% higher than the average $\bar{C}_{Optimal}$, whereas the benchmark controller is 38.5% higher than the average $\bar{C}_{Optimal}$.

8. Fuel gas consumer dynamics

As discussed in Section 2.1, the benchmark problem does not include consumer dynamics. To evaluate the NMPC performance in the presence of consumer dynamics, the consumer model described in Section 2.3 was added to the benchmark model. The NMPC used in Section 7 for the benchmark problem ($NMPC_1$) is compared to an NMPC that accounts for the effects of consumer dynamics in its state function ($NMPC_2$).

8.1. Including consumer dynamics in the NMPC model

The state vector in (16a) is amended to include $F_{FG_{Demand}}$ as a state: $\mathbf{x} = [\hat{N}_1, \hat{N}_2, \hat{N}_3, \hat{N}_4, \hat{N}_5, \hat{N}_6, F_{FG_{Demand}}]^T$. The consumer dynamics model was given as (8) in Section 2.3.

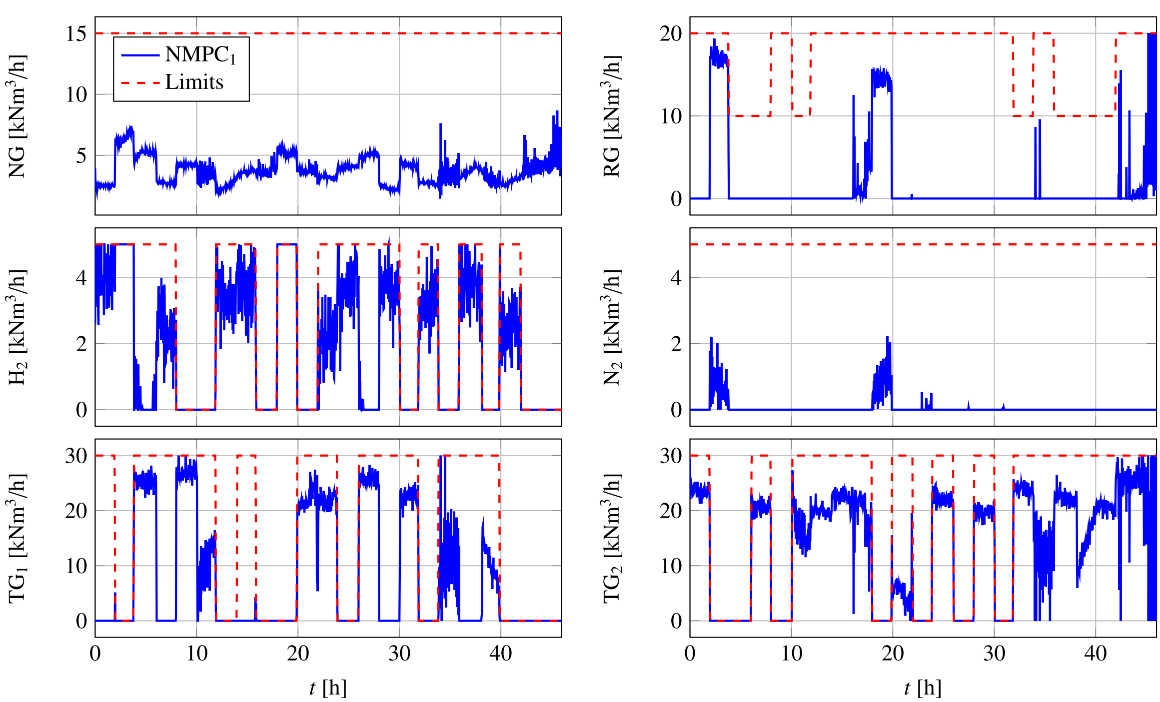

Fig. 5. NMPC MVs for benchmark case 1.

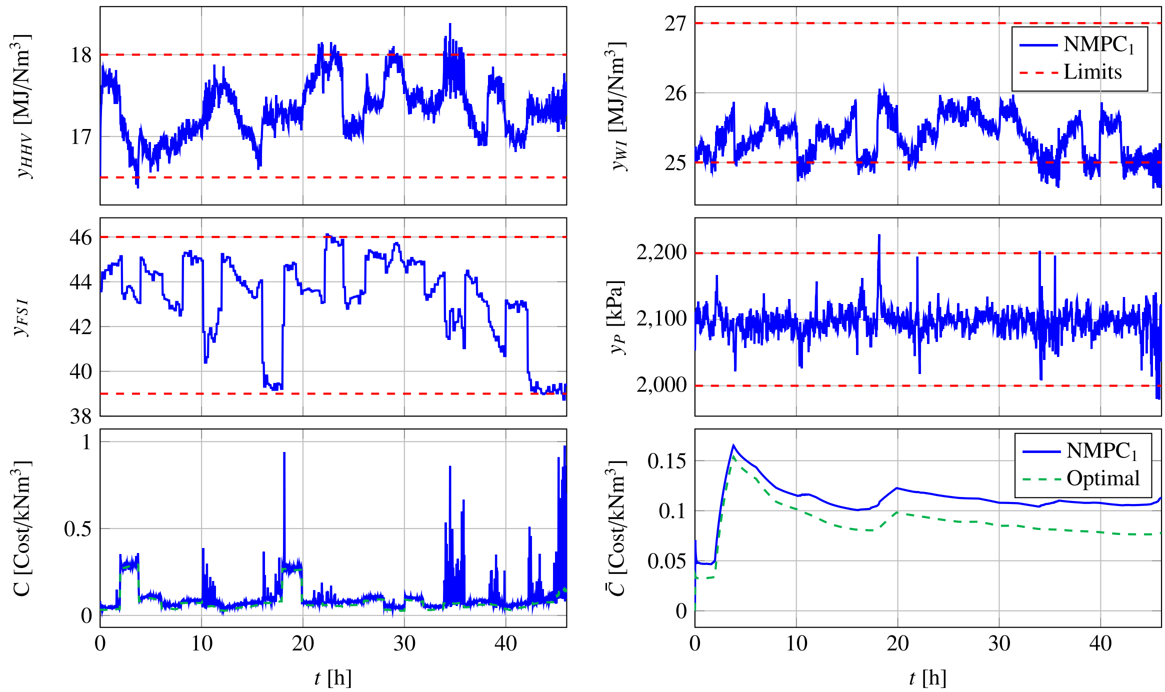

Fig. 6. NMPC CVs and costs for benchmark case 1.

Table 7
Comparison of final NMPC economic performance against benchmark results [11]. $\bar{C}$ (% higher than optimal cost), $\bar{C}_\delta$ (% contribution to total cost).

		NMPC	Benchmark[a]	Optimal[a]
Case 1	$\bar{C}$	0.1132 (45.1%)	0.1331 (70.6%)	0.078
	$\bar{C}_\delta$	0.0173 (15.3%)	0.0316 (23.7%)	0
Case 2	$\bar{C}$	0.1128 (29.7%)	0.1036 (19.1%)	0.087
	$\bar{C}_\delta$	0.0100 (8.9%)	0.0048 (4.6%)	0
Case 3	$\bar{C}$	0.0941 (27.2%)	0.0944 (27.6%)	0.074
	$\bar{C}_\delta$	0.0033 (3.5%)	0.0074 (7.8%)	0
Average	$\bar{C}$	0.1067 (33.9%)	0.1104 (38.5%)	0.0797
	$\bar{C}_\delta$	0.0102 (9.6%)	0.0146 (13.2%)	0

[a] Results reported in [11].

8.2. Case 4: Including consumer dynamics

The cases presented in the benchmark do not provide scenarios where the effects of consumer dynamics would affect the controller performance. As shown by [12], the largest model–plant mismatches relate to the models involving the NG and N_2 streams. Therefore, the largest difference would be noticed when there is a limitation of the other streams and the controller is forced to use NG and N_2 to meet $F_{FG_{Demand}}$ and maintain specifications.

The case below is created to show scenarios that would require the use of NG and N_2. The case starts at the nominal plant conditions with all streams available. The following events then take place at the specified times:

- 2 h: TG$_2$ availability drops from 30 to 19 kNm^3/h.
- 4 h: RG and TG$_1$ availability drops to 0 kNm^3/h.
- 6 h: TG$_1$ availability increases to 16.5 kNm^3/h.
- 8 h: TG$_2$ availability drops to 0 kNm^3/h.
- 10 h: RG availability increases to 16 kNm^3/h.
- 12 h: TG$_1$ availability drops to 0 kNm^3/h.
- 14 h: All streams are available at maximum capacity.

The above listed events represent scenarios where just enough RG, TG$_1$ or TG$_2$ would be available to make up the bulk of the fuel gas, and the controller maximises H_2, but must still use more NG and N_2 to meet demand. The lack of fuel gas supply or increase in demand is a common occurrence in an industrial plant when some of the units that provide off-gasses are not available and the fuel gas demand cannot be met without using more expensive streams.

8.3. Case 4 results

Figs. 7 and 8 shows the response of NMPC$_1$ and NMPC$_2$ for the consumer dynamics case. Both NMPCs behave similarly if there is enough availability of RG, TG$_1$ and/or TG$_2$. However, once there is a large offset between supply and demand, NMPC$_1$ aims to use more of the less expensive N_2 than NG to meet the demand. Since N_2 has no heating value, this action will also increase $F_{FG_{Demand}}$ [12], causing y_P to further drop and the controller to use more N_2. The control actions of NMPC$_1$ ultimately result in instability through oscillations as the controller is not able to maintain the pressure and the specifications within the required limits. NMPC$_2$ which accounts for consumer dynamics correctly uses more of the expensive NG and is able to meet $F_{FG_{Demand}}$ and reach a feasible solution which maintains all the fuel gas specifications within limits.

Table 8 shows the final $\bar{C}$ for case 4 as well as the contributions of $\bar{C}_c$ and $\bar{C}_\delta$ to the final $\bar{C}$. NMPC$_1$ has a total cost of 1.8831 which is significantly higher than the total cost of NMPC$_2$ of 0.1044. The cost $\bar{C}_\delta$,

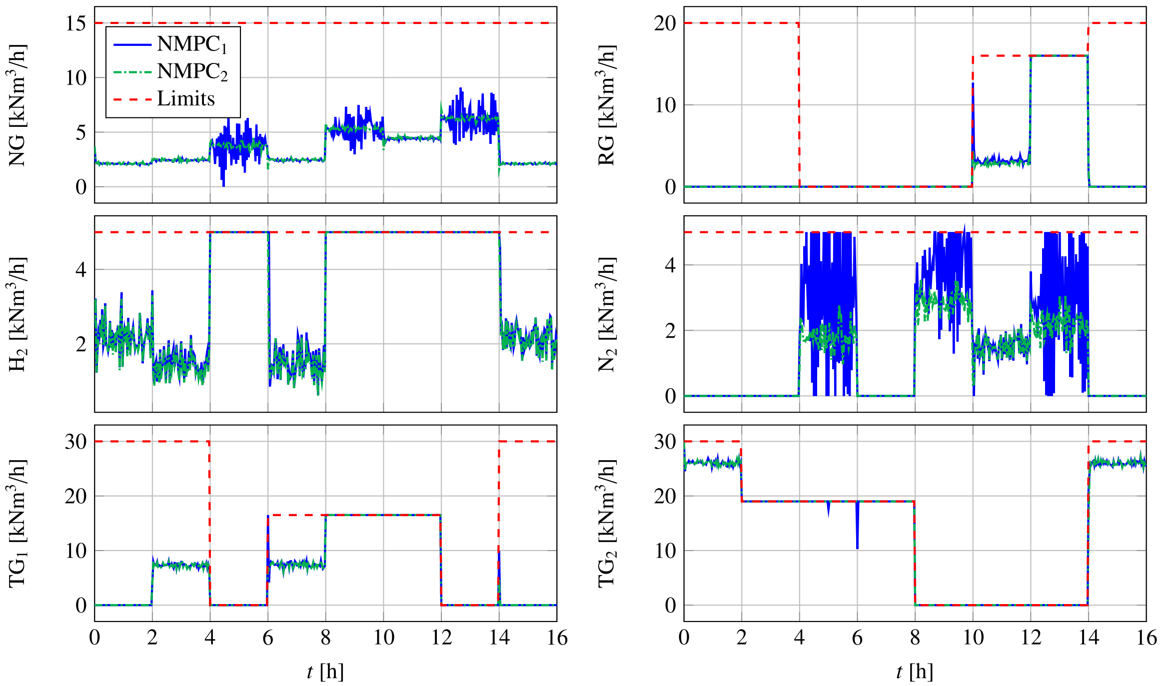

Fig. 7. NMPC$_1$ vs. NMPC$_2$ MVs during scenarios of limited feed streams.

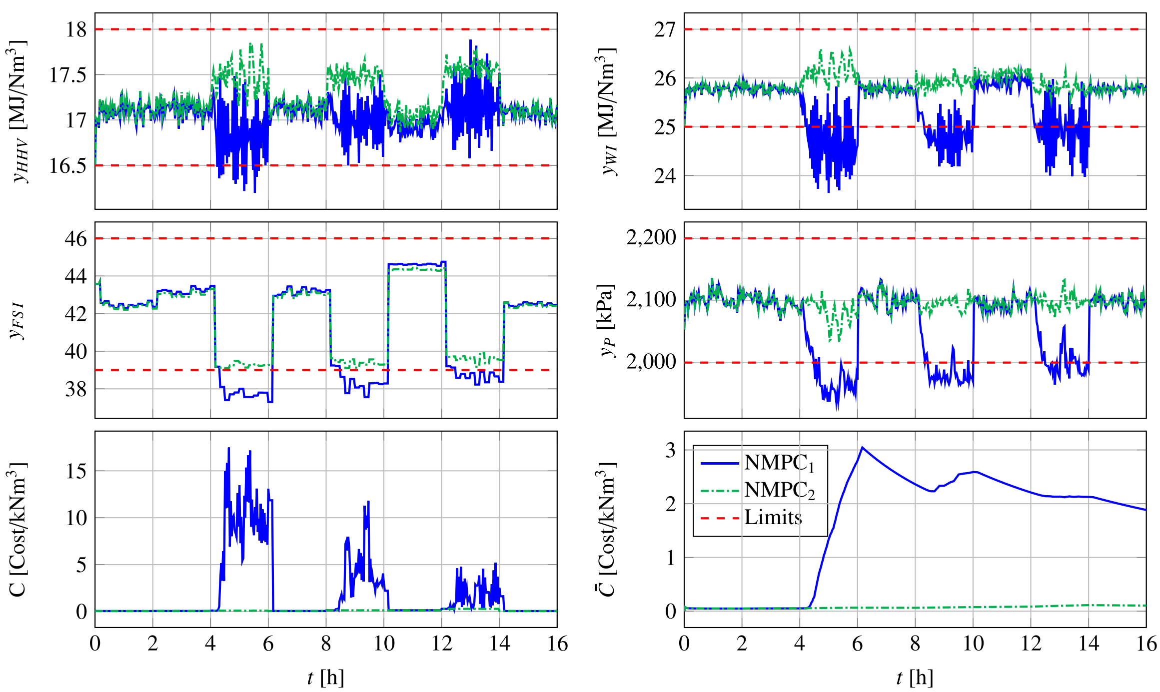

Fig. 8. NMPC$_1$ vs. NMPC$_2$ CVs and costs during scenarios of limited feed streams.

which indicates specification violations, contributes 94.4% of the total cost for NMPC$_1$ compared to 0% for NMPC$_2$. This is because NMPC$_2$ was able to maintain the CVs within their limits.

The excessive oscillations on the fuel gas heating value and other specifications caused by NMPC$_1$ will result in all equipment that use fuel gas in the plant to also oscillate. Furthermore, oscillations in the fuel gas controller causes factory-wide instabilities that could feed back into the fuel gas and amplify the problem even more. The oscillating behaviour can also result in operators typically switching off the controller more frequently and adjusting the available streams flow rates manually or using the base-layer control schemes. Switching off the controller results in sub-optimal operations considering costs and specification violations.

9. Conclusion

An NMPC was built for the fuel gas blending benchmark problem given by [11]. The NMPC uses an accurate continuous fuel gas header composition estimator designed using an EKF and MHE for the system. The estimated composition was used as states for the NMPC and to provide a continuous estimation for y_{FSI}. The state equation for the estimator was the mass balance equation of the header, and the

Table 8
Comparison of $NMPC_1$ vs. $NMPC_2$ results. $\bar{C}_\delta$ (% contribution to total cost).

		$NMPC_1$	$NMPC_2$
Case 4	$\bar{C}$	1.8831	0.1044
	$\bar{C}_c$	0.1049	0.1044
	$\bar{C}_\delta$	1.7775 (94.4%)	0 (0%)

estimations are updated every 10 min when a new analyser update becomes available.

The aim of the NMPC was to achieve improved performance compared to the benchmark controller. Overall, the NMPC achieved a cost 33.9% higher than the averaged optimal cost, whereas the benchmark controller achieved a cost 38.5% higher. The improved performance is largely a contribution from the first case since case 2 provided a poorer performance and case 3 provided a slightly better performance compared to the benchmark controller.

Consumer dynamics were added to the non-linear fuel gas model to make it more representative of a real process. A new case which has scenarios that force the controller to make a trade-off between using more of either NG or N_2 was investigated which would occur if there is limited off-gas supply or a large increase in fuel gas demand. The lack of fuel gas supply or increase in demand represents a common occurrence in industrial plants, especially when some of the units that provide off-gasses are not available and the fuel gas demand cannot be met without using more expensive streams.

It was shown that if the NMPC excludes consumer dynamics in the state function ($NMPC_1$), it could become unstable and result in oscillations and large specification violations during these periods. These oscillations would typically result in factory-wide instabilities as all equipment that use fuel gas would also oscillate. $NMPC_2$ which accounts for consumer dynamics provided stable control during these periods. For the new case, $NMPC_1$ achieved a total cost of 1.8831, of which 94.4% of the total cost was due to specification violations. $NMPC_2$ achieved a total cost of 0.1044 of which the penalty due to specification violations was 0%. Future work can include investigating offset-free mechanisms [23–25] on $NMPC_1$ to handle the consumer dynamics mismatches.

CRediT authorship contribution statement

M.D. Sibiya: Writing – original draft, Visualization, Validation, Methodology, Investigation, Formal analysis, Conceptualization. **A.J. Wiid:** Writing – review & editing, Supervision, Methodology, Conceptualization. **J.D. le Roux:** Writing – review & editing, Supervision, Methodology, Conceptualization. **I.K. Craig:** Writing – review & editing, Supervision, Methodology, Conceptualization.

Declaration of competing interest

The authors declare that they have no known competing financial interests or personal relationships that could have appeared to influence the work reported in this paper.

Data availability

No data was used for the research described in the article.

References

[1] M. Chaczykowski, P. Zarodkiewicz, Simulation of natural gas quality distribution for pipeline systems, Energy 134 (2017) 681–698.
[2] A.J. Wiid, J.D. le Roux, I.K. Craig, Modelling of methane-rich gas pipeline networks for simulation and control, J. Process Control 92 (2020) 234–245.
[3] A.J. Wiid, J.D. le Roux, I.K. Craig, Pressure measurement location selection in industrial gas headers for buffering control, Comput. Chem. Eng. 145 (2021) 107178.
[4] A.J. Wiid, J.D. le Roux, I.K. Craig, Pressure buffering control to reduce pollution and improve flow stability in industrial gas headers, Control Eng. Pract. 115 (2021) 104904.
[5] A. Arya, R. Katiyar, P. Kumar, A. Kapoor, D. Pal, G. Rangasamy, A multi-objective model for optimizing hydrogen injected-high pressure natural gas pipeline networks, Int. J. Hydrog. Energy 48 (2023).
[6] R. Dzedzemane, A.J. Wiid, J.D. le Roux, I.K. Craig, Natural gas well production network state-space model development and validation for process control, Ind. Eng. Chem. Res. 63 (3) (2024) 1461–1473.
[7] R.P. Dreyer, G.D. Kotze, Methods, systems, and articles for controlling a fluid blending system, 2007, US Patent 7, 188, 637.
[8] K.S. Brooks, A. Carr, R.P. Dreyer, M. Maksa, Energy and emissions optimisation at Chevron Cape Town, IFAC Proc. Vol. 47 (3) (2014) 1278–1283.
[9] M. Segers, P. Cannon, C. Gutierrez, B. Binkowski, Blending fuel gas to optimize use of off-spec natural gas, in: ISA Power Industry Division 54th Annual I&C Symposium, 2011.
[10] C.J. Muller, I.K. Craig, N.L. Ricker, Modelling, validation, and control of an industrial fuel gas blending system, J. Process Control 21 (6) (2011) 852–860.
[11] N.L. Ricker, C.J. Muller, I.K. Craig, Fuel gas blending benchmark for economic performance evaluation of advanced control and state estimation, J. Process Control 22 (6) (2012) 968–974.
[12] M.D. Sibiya, A.J. Wiid, J.D. le Roux, I.K. Craig, Modelling of consumer dynamics to improve fuel gas blending control, IFAC-PapersOnLine 58 (25) (2024) 67–72.
[13] M. Masoumi, Z. Izakmehri, Improving of refinery furnaces efficiency using mathematical modeling, Int. J. Model. Optim. 1 (2011) 74–79.
[14] C.V. Rao, J.B. Rawlings, J.H. Lee, Constrained linear state estimation—a moving horizon approach, Automatica 37 (10) (2001) 1619–1628.
[15] C.V. Rao, J.B. Rawlings, Constrained process monitoring: Moving-horizon approach, AIChE J. 48 (1) (2002) 97–109.
[16] C.C. Qu, J. Hahn, Computation of arrival cost for moving horizon estimation via unscented Kalman filtering, J. Process Control 19 (2) (2009) 358–363.
[17] S. Ungarala, Computing arrival cost parameters in moving horizon estimation using sampling based filters, J. Process Control 19 (9) (2009) 1576–1588.
[18] R. López-Negrete, S.C. Patwardhan, L.T. Biegler, Constrained particle filter approach to approximate the arrival cost in Moving Horizon Estimation, J. Process Control 21 (6) (2011) 909–919.
[19] R. López-Negrete, L.T. Biegler, A moving horizon estimator for processes with multi-rate measurements: A nonlinear programming sensitivity approach, J. Process Control 22 (4) (2012) 677–688.
[20] G. Sánchez, M. Murillo, L. Giovanini, Adaptive arrival cost update for improving Moving Horizon Estimation performance, ISA Trans. 68 (2017) 54–62.
[21] X. Li, X. Yin, A recursive approach to approximate arrival costs in distributed Moving Horizon Estimation, IFAC-PapersOnLine 58 (18) (2024) 257–262.
[22] A. Bemporad, N.L. Ricker, M. Morari, Model Predictive Control Toolbox^{TM} User's Guide, The MathWorks, Inc, 2024.
[23] M. Morari, U. Maeder, Nonlinear offset-free model predictive control, Automatica 48 (9) (2012) 2059–2067.
[24] G. Pannocchia, M. Gabiccini, A. Artoni, Offset-free mpc explained: novelties, subtleties, and applications, IFAC-PapersOnLine 48 (2015).
[25] H. Zhang, E. Prempain, A non-linear offset-free model predictive control design approach, Actuators 13 (8) (2024).